Reactivity of $SiMe_3$- and SnR_3-Functionalized Bis(7-azaindol-1-yl)methane with $[PtR_2(\mu\text{-}SMe_2)]_n$ (R = Me, Ph) and the Resulting Pt(II) and Pt(IV) Complexes

Shu-Bin Zhao, Rui-Yao Wang, and Suning Wang*

Department of Chemistry, Queen's University Kingston, Ontario K7L 3N6, Canada

Received January 11, 2009

Three new bis(7-azaindol-1-yl)methane (BAM) derivative ligands Me_3Si-BAM (**1a**), Me_3Sn-BAM (**1b**), and Ph_3Sn-BAM (**1c**) have been synthesized, and their reactivities with $[PtR_2(\mu\text{-}SMe_2)]_n$ (R = Me, Ph) have been examined. Two Pt(II) complexes Pt(Me_3Si-BAM)R_2 (R = Me, **2**; Ph, **3**) were obtained from the reactions of **1a**. The reactions of **1b** with $[PtR_2(\mu\text{-}SMe_2)]_n$ (R = Me, Ph) produced unexpected novel *N*,*C*,*N*-BAM Pt(IV) complexes Pt(*N*,*C*,*N*-BAM)($SnMe_3$)R_2 (R = Me, **4**; Ph, **6**) likely via oxidative cleavage of the C_{BAM}−Sn bond in **1b**. **1c** reacted with $[PtPh_2(\mu\text{-}SMe_2)]_n$ (n = 2, 3) yielding the anticipated Pt(II) complex Pt(Ph_3Sn-BAM)Ph_2 (**7**), whereas its reaction with $[PtMe_2(\mu\text{-}SMe_2)]_2$ resulted in unusual Pt^{II}-*Me* and Sn^{IV}-*Ph* metathesis, yielding also **7** as one of the products. Mechanistic investigation was carried out to understand this phenomenon. The reactivities of **2** with MeI, MeOTf, and I_2 were examined. Its reaction with I_2 gave rise to Pt(Me_3Si-BAM)I_2 (**9**) along with CH_3I, indicating the possibility of functionalizing Pt^{II}-*Me* via iodinolysis. The reaction of Pt(*N*,*C*,*N*-BAM)($SnMe_3$)Me_2 (**4**) with I_2 produced a number of unusual *N*,*C*,*N*-BAM Pt(IV) complexes including Pt(*N*,*C*,*N*-BAM)Me(I)(SnI_2Me) (**13**) and Pt(*N*,*C*,*N*-BAM)Me(I)(I_3) (**14**) due to the electrophilic cleavage of the Sn-Me, Pt-Me and/or Pt−Sn bond(s) by I_2. For comparison, we also investigated the reaction of Pt(*N*,*C*,*N*-BAM)Me_3 (**M1**) with I_2 which was found to exhibit a high regioselectivity for the axial Pt-Me group, resulting in Pt(*N*,*C*,*N*-BAM)$Me_2(I_3)$ (**15**) with the two Pt-*Me* being *cis* to each other. The reactions of **4** and **M1** with I_2 are rare examples of Pt^{IV}−CH_3 bond cleavage by the elimination of CH_3I. The structures of **1a** and complexes **2**, **7**, **9**, and **13**−**15** were determined by X-ray diffraction analyses.

Introduction

Design and syntheses of N,N-chelating ligands represent a theme in transition-metal chemistry, at least partly attributable to a number of their distinct practical merits, such as being stable, broadly available, highly modular, and amenable to a variety of derivatization techniques. N,N-Chelating ligands have also played a unique role in advancing the Shilov chemistry.[1] We previously developed several 7-azaindolyl derivative N,N-chelating ligands, which gave unusual boat-shaped Pt(II) complexes capable of cleaving C−H bonds under mild conditions.[2] Meanwhile, the geometry of these ligands not only allowed the isolation of rare reaction intermediates[2a] but promoted unique reactivities of the complexes, such as distinct C−H activation-driven self-assembly,[3] multiple benzene C−H activation,[4a] double C−Cl bond activation,[4b] and unprecedented diastereoselectivity in ethylbenzene C−H activation.[2b] Recently, to examine the influences of ligand chelating ring size on the stability and reactivity of Pt(II) centers, we developed several new bis(7-azaindol-1-yl) ligands with various linker groups.[5]

Pt^{IV} chemistry has drawn enormous attention over the last two decades toward tackling the functionalization step in the Shilov processes,[1,6] especially after Puddephatt, Goldberg, et al. demonstrated experimentally that five-coordinate cationic Pt^{IV} complexes are often inevitably involved as key intermediates along the reaction coordinates for Pt^{II}/Pt^{IV}-mediated C−X (X = H, halide, OR, etc.) bond-breaking or -making processes.[6−10] Remarkably, such coordinative unsaturated Pt(IV) species were recently found to be isolable by applying bulky anionic N,N-chelating ligands.[8−10] During the course of our work on Pt(IV) chemistry, we have shown that certain neutral ligands can also promote the formation of the five-coordinate Pt(IV) cation if sufficient steric protection can be provided to the Pt(IV) vacant coordination site.[11] Despite being five-coordinate in solution, due to the inadequate steric protection from the bis(7-azaindol-1-yl)methane (BAM) ligand, its Pt(IV) complexes exist preferentially as six-coordinate in solid state via bonding either with the OTf (OTf = $CF_3SO_3^-$) counterion or a THF molecule.[11] However, we found that the BAM bridging methylene group can be selectively deprotonated by either LDA or *n*-BuLi to give rise to the bis(7-azaindol-1-yl)methyl lithium salt, which reacted with $[Pt^{IV}Me_3(THF)](PF_6)$ in situ resulting in a stable

* To whom correspondence should be addressed. E-mail: wangs@chem.queensu.ca.

(1) For recent comprehensive reviews, see: (a) Goldberg, K. I.; Goldman, A. S. *Activation and Functionalization of C−H Bonds*; American Chemical Society: Washington, DC, 2004. (b) Lersch, M.; Tilset, M. *Chem. Rev.* **2005**, *105*, 2471. (c) Labinger, J. A.; Bercaw, J. E. *Nature (London)* **2002**, *417*, 507.

(2) (a) Zhao, S.-B; Wu, G.; Wang, S. *Organometallics* **2006**, *25*, 5979. (b) Zhao, S.-B.; Song, D; Jia, W.-L.; Wang, S. *Organometallics* **2005**, *24*, 3290. (c) Song, D.; Wang, S. *Organometallics* **2003**, *22*, 2187.

(3) Zhao, S.-B.; Wang, R.-Y.; Wang, S. *J. Am. Chem. Soc.* **2007**, *129*, 3092.

(4) (a) Song, D.; Jia, W.-L.; Wang, S. *Organometallics* **2004**, *23*, 1194. (b) Song, D.; Sliwowski, K.; Pang, J.; Wang, S. *Organometallics* **2002**, *21*, 4978.

(5) Zhao, S.-B.; Liu, G.-H.; Song, D.; Wang, S. *Dalton Trans.* **2008**, 6953.

(6) (a) Puddephatt, R. J. *Angew. Chem., Int. Ed.* **2002**, *41*, 261. (b) Roy, S.; Puddephatt, R. J.; Scott, J. D. *J. Chem. Soc., Dalton Trans.* **1989**, 2121. (c) Brown, M. P.; Puddephatt, R. J.; Upton, C. E. E. *J. Chem. Soc., Dalton Trans.* **1974**, 2457.

10.1021/om900022n CCC: $40.75
Publication on Web 04/01/2009

Chart 1

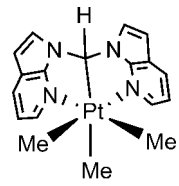

M1

six-coordinate *fac*-Pt^{IV}Me$_3$ complex **M1** (Chart 1), in which BAM adopted a novel κ^3-N,C,N coordination mode.[11]

We also envisioned that this lithium salt may be used to derivatize and functionalize the BAM ligand. To advance our study on Pt(IV) chemistry, we recently attempted to decorate the BAM methylene carbon with organometallic functional groups of heavier group 14 elements, as ligands incorporating the Si/Sn functionalities frequently exhibit diverse and distinct reactivity when bound with transition metals.[12] In addition, the bulky groups installed in these derivatives may provide a better steric protection for five-coordinate Pt^{IV} complexes, thus allowing subsequent reactivity studies. In this contribution, we present three new ligands obtained by functionalizing the BAM bridging methylene group with SiMe$_3$ and SnR$_3$ (R = Me, Ph) and our findings on the distinct reactivities of these new BAM derivative ligands with [PtR$_2$(μ-SMe$_2$)]$_n$ (R = Me, Ph) as well as the rather unusual reactivities of the resulting Pt(II) and the unexpected Pt(IV) heterodinuclear complexes when treated with electrophiles.

Experimental Section

All reactions were performed under N_2 with the standard Schlenk techniques unless otherwise noted. All starting materials were purchased from Aldrich Chemical Co. and used without further purification. THF, Et_2O, and hexanes were purified using the solvent purification system (Innovation Technology, Inc.), and CH_2Cl_2 was freshly distilled over P_2O_5. Deuterated solvents (Cambridge Isotopes) were used as received unless otherwise noted. NMR spectra were recorded on Bruker Advance 400 or 500 MHz spectrometers. Elemental analyses were performed by Canadian Microanalytical Service, Ltd., Delta, British Columbia. High-resolution mass spectra (HRMS) were obtained from a Waters/Micromass GC-TOF EI-MS spectrometer. Complexes Pt(*N*,*C*,*N*-BAM)PtMe$_3$,[11] [PtPh$_2$(μ-SMe$_2$)]$_n$ (n = 2 or 3),[13a] and [PtMe$_2$(μ-SR$_2$)]$_2$ (R = Me, Et)[13b] were prepared by methods described in the literature.

Synthesis of Me$_3$Si-BAM (1a). To a stirred Et_2O (20 mL) solution of bis(7-azaindol-1-yl)methane (0.25 g, 1.0 mmol) at −78 °C was added dropwise, via syringe, a *n*-BuLi solution (1.6 M) (0.75 mL, 1.2 mmol) over 5 min, and the resulting light yellow solution was stirred for 30 min at −78 °C. Me_3SiCl (1.0 mL, 7.9 mmol) was then slowly added via syringe. After being kept at −78 °C for additional 30 min, the reaction mixture was warmed to room temperature and stirred overnight. After removal of the solvent, the residue was purified by flash chromatography on silica gel using CH_2Cl_2 as the eluent to afford **1a** as a white solid (0.18 g, 55% yield). Colorless crystals of **1a** were obtained via slow evaporation of its hexane solution. ^{1}H NMR (500 Hz, $CDCl_3$, 25 °C): δ 8.40 (d; ^3J = 2.0 Hz; 2H, 7-aza), 7.89 (d; ^3J = 6.0 Hz; 2H, 7-aza), 7.72 (d; ^3J = 2.0 Hz; 2H, 7-aza), 7.07 (m; 2H, 7-aza), 6.41 (d; ^3J = 2.0 Hz; 2H, 7-aza), 3.10 (br; 1H, bridging C*H*SiMe$_3$), 0.31 (s; 9H, Si*Me*$_3$) ppm. ^{13}C NMR: δ 148.06, 143.07, 129.72, 129.04, 120.77, 116.48, 100.66, 57.43, −0.80 ppm. HRMS: calcd for [$C_{18}H_{20}N_4Si$ + Na^+] 343.1355, found 343.1352.

Synthesis of Me$_3$Sn-BAM (1b). To a stirred THF (10 mL) solution of bis(7-azaindol-1-yl)methane (0.20 g, 0.81 mmol) at −78 °C was added dropwise, via syringe, an *n*-BuLi solution (1.6 M) (0.75 mL, 1.2 mmol) over 5 min, and the resulting light yellow solution was stirred for 30 min at −78 °C. A THF (5 mL) solution of Me_3SnCl (0.28 g, 1.4 mmol) was then slowly added via syringe. After being kept at −78 °C for an additional 30 min, the reaction mixture was warmed to room temperature and stirred overnight. After the removal of the solvent, the residue was purified by flash chromatography on silica gel using CH_2Cl_2/hexanes (1:1) as the eluent to afford **1b** as a colorless oil (0.24 g, 72% yield). ^{1}H NMR (500 Hz, $CDCl_3$, 25 °C): δ 8.36 (d; ^3J = 5.0 Hz; 2H, 7-aza), 7.90 (d; ^3J = 7.5 Hz; 2H, 7-aza), 7.48 (br; 2H, 7-aza), 7.10 (dd; $^3J_1$ = 5.0 Hz, $^3J_2$ = 7.5 Hz; 2H, 7-aza), 6.97 (s, satellites;$^2J_{Sn-H}$ = 43.9; 1H, bridging C*H*SnMe$_3$), 6.38 (d; ^3J = 3.5 Hz; 2H, 7-aza), 0.26 (s;$^2J_{Sn-H}$ = 54.5 Hz; 9H, CHSn*Me*$_3$) ppm. ^{13}C NMR: δ 148.07, 142.44, 129.94, 129.32, 120.91, 116.38, 100.63, 53.89, −5.06 ($^1J_{Sn-C}$ = 353.9 Hz) ppm. ^{119}Sn NMR (186 Hz, CD_2Cl_2, 25 °C): δ −7.31 ppm. HRMS: calcd for [$C_{18}H_{20}N_4Sn$ + Na^+] 435.0608, found 435.0603.

Synthesis of Ph$_3$Sn-BAM (1c). This ligand was obtained as a white solid in 59% yield by a similar method as described above for **1b**, using Ph_3SnCl instead of Me_3SnCl. ^{1}H NMR (400 Hz, CD_2Cl_2, 25 °C): δ 8.16 (dd; ^3J = 4.8 Hz, ^4J = 1.2 Hz; 2H, 7-aza), 7.91 (dd; ^3J = 8.0 Hz, ^4J = 1.2 Hz; 2H, 7-aza), 7.80 (d; ^3J = 3.2 Hz; 2H, 7-aza), 7.51 (m, satellites; $^3J_{Sn-H}$ = 49.6 Hz; 6H, Ph), 7.25−7.21 (m; 9H, Ph), 7.10 (dd; $^3J_1$ = 4.8 Hz, $^3J_2$ = 8.0 Hz; 2H, 7-aza), 7.03 (s, satellites;$^2J_{Sn-H}$ = 58.0; 1H bridging C*H*SnPh$_3$) 6.44 (d; ^3J = 3.2 Hz; 2H, 7-aza) ppm. ^{13}C NMR: δ 147.27, 141.91, 136.70, 130.24 (br), 129.49, 128.97 (br), 128.33, 128.03, 120.57, 116.24, 100.55, 65.65 ppm. HRMS: calcd for [$C_{33}H_{26}N_4Sn$ + Na^+] 621.1077, found 621.1124.

Synthesis of Pt(Me$_3$Si-BAM)Me$_2$ (2). Ligand **1a** (0.064 g, 0.20 mmol) and [PtMe$_2$(μ-SMe$_2$)]$_2$ (0.057 g, 0.10 mmol) were mixed in dry THF (10 mL), and the mixture was stirred overnight at room temperature. The solvent was evaporated, and the resulting white solid was then washed with Et_2O (2 mL × 3) to afford **2** as a white powder (0.074 g, 68% yield). Colorless crystals of **2** were obtained from the slow evaporation of its THF solution. ^{1}H NMR (500 Hz,

(7) (a) Pawlikowski, A. V.; Getty, A. D.; Goldberg, K. I. *J. Am. Chem. Soc.* **2007**, *129*, 10382. (b) Procelewska, J.; Zahl, A.; Liehr, G.; van Eldik, R.; Smythe, N. A.; Williams, B. S.; Goldberg, K. I. *Inorg. Chem.* **2005**, *44*, 7732. (c) Crumpton-Bregel, D. M.; Goldberg, K. I. *J. Am. Chem. Soc.* **2003**, *125*, 9442. (d) Jensen, M. P.; Wick, D. D.; Reinartz, S.; White, P. S.; Templeton, J. L.; Goldberg, K. I. *J. Am. Chem. Soc.* **2003**, *125*, 8614. (e) Williams, B. S.; Goldberg, K. I. *J. Am. Chem. Soc.* **2001**, *123*, 2576. (f) Crumpton, D. M.; Goldberg, K. I. *J. Am. Chem. Soc.* **2000**, *122*, 962. (h) Williams, B. S.; Holland, A. W.; Goldberg, K. I. *J. Am. Chem. Soc.* **1999**, *121*, 252.

(8) (a) Fekl, U.; Kaminsky, W.; Goldberg, K. I. *J. Am. Chem. Soc.* **2003**, *125*, 15286. (b) Fekl, U.; Goldberg, K. I. *J. Am. Chem. Soc.* **2002**, *124*, 6804.

(9) (a) Luedtke, A. T.; Goldberg, K. I. *Inorg. Chem.* **2007**, *46*, 8496. (b) Kloek, S. M.; Goldberg, K. I. *J. Am. Chem. Soc.* **2007**, *129*, 3460. (c) Fekl, U.; Kaminsky, W.; Goldberg, K. I. *J. Am. Chem. Soc.* **2001**, *123*, 6423.

(10) Reinartz, S.; White, P. S.; Brookhart, M.; Templeton, J. L. J. *Am.Chem. Soc.* **2001**, *123*, 6425.

(11) Zhao, S.-B; Wu, G.; Wang, S. *Organometallics* **2008**, *27*, 1030.

(12) For selected examples of ligand systems incorporating Si functionalities (a−f) or Sn functionalities (g−j), see: (a) Sangtrirutnugul, P.; Tilley, T. D. *Organometallics* **2008**, *27*, 2223. (b) Sangtrirutnugul, P.; Tilley, T. D. *Organometallics* **2007**, *26*, 5557. (c) Sangtrirutnugul, P.; Stradiotto, M.; Tilley, T. D. *Organometallics* **2006**, *25*, 1607. (d) Stradiotto, M.; Fujdala, K.; Tilley, T. D. *Chem. Commun.* **2001**, *13*, 1200. (e) Stradiotto, M.; Hazendonk, P.; Bain, A. D.; Brook, M. A.; McGlinchey, M. J. *Organometallics* **2000**, *19*, 590. (f) Xie, Y.-F.; Wen, Z.-K; Tan, R.-Y.; Hong, J.; Zhao, S.-B.; Tang, L.-F. *Organometallics* **2008**, *27*, 5684. (g) Wen, Z.-K.; Xie, Y.-F.; Zhao, S.-B.; Tan, R.-Y.; Tang, L.-F. *J. Organomet. Chem.* **2008**, *693*, 1359. (h) Zhang, X.-Y.; Hong, J.; Song, H.-B.; Tang, L.-F. *Organometallics* **2007**, *26*, 4038. (i) Tang, L.-F.; Zhao, S.-B.; Jia, W.-L.; Yang, Z.; Song, D.-T.; Wang, J.-T. *Organometallics* **2003**, *22*, 3290. (j) Tang, L.-F.; Jia, W.-L.; Song, D.-T.; Wang, Z.-H.; Chai, J.-F.; Wang, J.-T. *Organometallics* **2002**, *21*, 445.

(13) (a) Song, D.; Wang, S. *J. Organomet. Chem.* **2002**, *648*, 302–305. (b) Scott, J. D.; Puddephatt, R. J. *Organometallics* **1983**, *2*, 1643.

CD_2Cl_2, 25 °C): δ 13.13 (s, satellites; J_{Pt-H} = 61.0 Hz; 1H, C*H*SiMe$_3$), 8.72 (d; ^3J = 5.5; 2H, 7-aza), 7.96 (d;^3J = 8.0; 2H, 7-aza), 7.56 (d;^3J = 3.5; 2H, 7-aza), 7.04 (dd; $^3J_1$ = 5.5 Hz, $^3J_2$ = 8.0 Hz; 2H, 7-aza), 6.59 (d;^3J = 3.5 Hz; 2H, 7-aza), 0.67 (s, satellites; $^2J_{Pt-H}$ = 88.0 Hz; 6H, Pt*Me*$_2$) 0.45 (s; 9H, CHSi*Me*$_3$) ppm. ^{13}C NMR: δ 146.51, 144.89, 129.25, 127.88, 123.24, 117.40, 102.21, 54.69, −1.79, −19.85 ($^1J_{Pt-H}$ = 838.6 Hz; Pt*Me*$_2$) ppm. Anal. Calcd for $C_{20}H_{26}N_4PtSi$: C, 44.03; H, 4.80; N, 10.27. Found: C, 44.37; H, 4.79; N, 9.88.

Synthesis of Pt(Me$_3$Si-BAM)Ph$_2$ (3). Ligand **1a** (0.032 g, 0.10 mmol) and [PtPh$_2$(μ-SMe$_2$)]$_n$ (n = 2, 3) (0.041 g, 0.10 mmol based on Pt) were mixed in THF (10 mL), and the mixture was stirred overnight at room temperature. The solvent was evaporated, and the resulting white solid was then washed with Et$_2$O (3 mL × 3) to afford **3** as a white powder (0.056 g, 84% yield). ^{1}H NMR (400 Hz, CD_2Cl_2, 25 °C): δ 12.60 (s, satellites; J_{Pt-H} = 44.1 Hz; 1H, C*H*SiPh$_3$), 8.75 (dd; ^3J = 5.5 Hz, ^4J = 1.2 Hz; 2H, 7-aza), 7.90 (dd; ^3J = 8.0 Hz, ^4J = 1.2 Hz; 2H, 7-aza), 7.65 (d; ^3J = 4.0 Hz; 2H, 7-aza), 7.41 (m, satellites; $^3J_{Pt-H}$ = 74.6 Hz; 4H, Ph), 6.98 (dd; $^3J_1$ = 5.5 Hz, $^3J_2$ = 8.0 Hz; 2H, 7-aza), 6.80 (m; 4H, Ph), 6.70 (m; 2H, Ph), 6.61 (d;^3J = 4.0 Hz; 2H, 7-aza) ppm. ^{13}C NMR: δ 146.37, 145.18, 142.56, 138.32, 130.23, 128.17, 126.52, 123.89, 121.68, 117.06, 102.72, 55.83, −0.95 ppm. Anal. Calcd for $C_{30}H_{30}N_4PtSi$: C, 53.80; H, 4.51; N, 8.37. Found: C, 53.64; H, 4.73; N, 8.30.

Synthesis of Pt(N,C,N-BAM)(SnMe$_3$)Me$_2$ (4). 1b (0.041 g, 0.10 mmol) and [PtMe$_2$(μ-SMe$_2$)] (0.057 g, 0.10 mmol) were mixed in dry CH_2Cl_2 (10 mL), and the mixture was stirred for 1 day at room temperature. After the solvent was decanted, the residue was purified by flash chromatography on silica gel using CH_2Cl_2/hexanes (1:1) as the eluent to afford **4** as a colorless oil in >90% yield. ^{1}H NMR (400 Hz, CD_2Cl_2, 25 °C): δ 8.32 (dd, satellites; ^3J = 5.6 Hz; 1H, 7-aza), 8.25 (dd; ^3J = 5.2 Hz, ^4J = 1.2 Hz; 1H, 7-aza), 7.90 (m; 2H, 7-aza), 7.58 (d; ^3J = 3.2 Hz; 1H, 7-aza), 7.53 (d; ^3J = 3.2 Hz; 1H, 7-aza), 7.08−7.01 (m; 2H, 7-aza), 6.76 (d; ^3J = 3.2 Hz; 1H, 7-aza), 6.73 (d; ^3J = 3.2 Hz; 1H, 7-aza), 5.99 (s, satellites; $^2J_{Pt-H}$ = 16.4 Hz; 1H, bridging C*H*), 0.73 (s, satellites; $^2J_{Pt-H}$ = 42.4 Hz; 3H, Pt-*Me*), 0.52 (s, satellites; $^2J_{Pt-H}$ = 64.4 Hz; 3H, Pt-*Me*), −0.25 (s, satellites; $^2J_{Sn-H}$ = 48.0 Hz, $^3J_{Pt-H}$ = 10.0 Hz; 9H, Pt−Sn*Me*$_3$) ppm. ^{13}C NMR (100 Hz, CD_2Cl_2, 25 °C): δ 154.76, 152.43, 139.28, 137.46, 129.96, 129.82, 129.21, 128.29, 119.70, 119.14, 115.91, 104.09, 103.48, 72.80 (s, satellites; $^1J_{Pt-C}$ = 483.7 Hz; bridging *C*H'-Pt), −8.33 (s, satellites; $^1J_{Pt-C}$ = 459.6 Hz, Pt-*Me*), −11.89 (s, satellites; $^1J_{Sn-C}$ = 65.6 Hz, Sn*Me*$_3$), −21.64 (s, satellites; $^1J_{Pt-C}$ = 316.3 Hz, Pt-*Me*) ppm. ^{119}Sn NMR (186 Hz, CD_2Cl_2, 25 °C): δ −84.42 ($^2J_{Pt-Sn}$ = 10728.7 Hz) ppm. HRMS: calcd for [$C_{20}H_{26}N_4PtSn$ + H$^+$] 637.0885, found 637.0805.

In Situ Syntheses of Pt(Me$_3$Sn-BAM)Ph$_2$ (5) and Pt(N,C,N-BAM)(SnMe$_3$)Ph$_2$ (6). An NMR tube was charged with Me$_3$Sn-BAM (**2**) (8.3 mg, 0.020 mmol) and [PtPh$_2$(μ-SMe$_2$)]$_n$ (n = 2, 3) (16.6 mg, 0.040 mmol based on Pt). CD_2Cl_2 (0.50 mL) was added via syringe at room temperature. The NMR tube was shaken to dissolve the solid, and the ^{1}H NMR spectra were monitored over two months. Diagnostic ^{1}H NMR (500 Hz, CD_2Cl_2, 25 °C) of **5**: δ 12.67 (s, satellites; $^2J_{Sn-H}$ = 55.1 Hz, J_{Pt-H} = 34.9 Hz; 1H, bridging C*H*), 8.75 (dd, satellites; ^3J = 5.0 Hz, ^4J = 1.0 Hz, $^3J_{Pt-H}$ = 21.6 Hz; 2H, 7-aza). Diagnostic ^{1}H NMR (500 Hz, CD_2Cl_2, 25 °C) of **6**: 6.33 (s, satellites; $^2J_{Pt-H}$ = 14. Hz; 1H, bridging C*H*), −0.30 (s, satellites; $^2J_{Sn-H}$ = 48.4 Hz,$^3J_{Pt-H}$ = 9.0 Hz; 9H, Sn*Me*$_3$) ppm.

Synthesis of Pt(Ph$_3$Sn-BAM)Ph$_2$ (7). Ph$_3$Sn-BAM (**1c**) (0.030 g, 0.05 mmol) and [PtPh$_2$(μ-SMe$_2$)]$_n$ (n = 2, 3) (0.040 g, 0.10 mmol based on Pt) were mixed in in CH_2Cl_2 (4 mL), and the mixture was stirred overnight at room temperature. The solvent was evaporated, and the resulting white solid was then recrystallized with CH_2Cl_2/hexanes (1:2) mixed solution to afford **7** as a white powder (0.036 g, 77% yield). ^{1}H NMR (500 Hz, CD_2Cl_2, 25 °C): δ 13.07 (s, satellites; J_{Pt-H} = 56.9 Hz; 1H, C*H*SnPh$_3$), 8.74 (dd; ^3J = 5.5 Hz, ^4J = 1.0 Hz; 2H, 7-aza), 7.90 (dd; ^3J = 7.5 Hz, ^4J = 1.0 Hz; 2H, 7-aza), 7.74 (m, satellites; $^3J_{Sn-H}$ = 51.0 Hz; 8H, 2H from 7-aza and 6H from Sn*Ph$_3$*), 7.50 (m; 3H, Sn*Ph$_3$*), 7.45 (m; 6H, Sn*Ph$_3$*), 7.21 (m, satellites; $^3J_{Pt-H}$ = 68.4 Hz; 4H, Pt*Ph$_2$*), 6.99 (dd; $^3J_1$ = 5.5 Hz, $^3J_2$ = 7.5 Hz; 2H, 7-aza), 6.65 (m; 6H, Pt*Ph$_2$*) ppm. ^{13}C NMR: δ 147.61, 142.25, 138.48, 137.69, 136.05, 133.98, 130.58, 130.50, 130.11, 126.54, 124.37, 121.56, 117.34, 103.10, 66.51 ppm. ^{119}Sn NMR (186 Hz, CD_2Cl_2, 25 °C): δ 0.75 ppm. Anal. Calcd for $C_{45}H_{36}N_4PtSn \cdot CH_2Cl_2$: C, 53.56; H, 3.71; N, 5.43. Found: C, 53.59; H, 3.86; N, 4.86.

Alternatively, allowing the solution of Ph$_3$Sn-BAM (**1c**) (16 mg, 0.026 mmol) and [PtMe$_2$(μ-SMe$_2$)]$_2$ (15 mg, 0.026 mmol) in CH_2Cl_2 (0.8 mL) to stand at room temperature in the dark resulted in colorless crystals of **7** (∼6 mg, 24% yield based on **1c**).

Reactivity Study of Pt(Me$_3$Si-BAM)Me$_2$ (2) with MeOTf. An ^{1}H NMR spectrum was first recorded for a dry CD_2Cl_2 (0.40 mL) (CD_2Cl_2 was dried with CaH_2 prior to use) solution of **2** (∼8 mg). MeOTf (1.7 μL, ∼1.05 equiv) was then added via micropipet at room temperature. The NMR tube was shaken vigorously for a few seconds, and then a new NMR spectrum of the solution was recorded. The ^{1}H NMR data indicated the clean formation of [Pt(Me$_3$Si-BAM)Me$_3$](OTf) (**8**). ^{1}H NMR (500 Hz, CD_2Cl_2, 25 °C): δ 8.41 (d; ^3J = 5.0 Hz; 2H, 7-aza), 8.20 (d; ^3J = 8.0 Hz; 2H, 7-aza), 7.65 (d; ^3J = 4.0 Hz; 2H, 7-aza), 7.40 (dd; $^3J_1$ = 5.0 Hz,$^3J_2$ = 8.0 Hz; 2H, 7-aza), 6.95 (d; ^3J = 4.0 Hz; 2H, 7-aza), 5.00 (s, satellites; J_{Pt-H} = 88.9 Hz; 1H, bridging C*H'*(SiMe$_3$)), 1.79 (s, satellites; $^2J_{Pt-H}$ = 73.5 Hz; 9H, Pt-*Me*), 0.55 (s; 9H, Si*Me$_3$*) ppm. ^{13}C NMR: δ 148.14, 142.09, 133.23, 127.97, 124.96, 118.92, 105.86, 65.89, −0.98, −6.53 ($^1J_{Pt-H}$ = 629 Hz; Pt-*Me*) ppm. Complex **8** decomposed completely after 3 days, resulting in the tetrameric complex [PtMe$_3$(OTf)]$_4$ via extrusion of ligand **1a**.

Reactivity Study of Pt(Me$_3$Si-BAM)Me$_2$ (2) with I$_2$. An ^{1}H NMR spectrum was first recorded for a CD_2Cl_2 (0.40 mL) solution of **2** (∼8 mg). I_2 (4 mg, ∼1.05 equiv) was then added at room temperature. After being shaken vigorously to dissolve I_2, the solution was monitored regularly by ^{1}H NMR over several days. The products generated were identified to be a mixture containing Pt(Me$_3$Si-BAM)(I)$_2$ (**9**), MeI (^{1}H, δ = 2.20 ppm), free ligand **1a**, and [PtMe$_3$I]$_4$ (^{1}H, δ = 1.73 ppm, $^2J_{Pt-H}$ = 77.2 Hz). Slow evaporation of the CD_2Cl_2 solution afforded yellow crystals, which were characterized by single-crystal X-ray diffraction analysis to be the co-crystallized product of complex **9** with [PtMe$_3$I]$_4$. ^{1}H NMR (500 Hz, CD_2Cl_2, 25 °C) of **9**: δ 12.89 (s, satellites; J_{Pt-H} = 50.0 Hz; 1H, C*H*SiMe$_3$), 9.01 (d; ^3J = 6.5 Hz; 2H, 7-aza) 8.00 (d; ^3J = 7.0 Hz; 2H, 7-aza), 7.64 (d; ^3J = 2.0 Hz; 2H, 7-aza), 7.16 (dd; $^3J_1$ = 6.5 Hz, $^3J_2$ = 7.0 Hz; 2H, 7-aza), 6.71 (d; ^3J = 2.0 Hz; 2H, 7-aza) ppm. The reaction of **2** (∼8 mg) with 3 equiv of I_2 (∼11 mg) in CD_2Cl_2 (0.40 mL) at room temperature gave similar results, again producing **9**, MeI, free ligand **1a**, and [PtMe$_3$I]$_4$. Slow evaporation of the CD_2Cl_2 solution afforded deep red crystals, which were characterized by single-crystal X-ray diffraction analysis to be the co-crystallized product of **9** with I_2. The X-ray data for the co-crystallized product of **9** with I_2 are provided in the Supporting Information.

Reactivity Study of Pt(*N*,*C*,*N*-BAM)(SnMe$_3$)Me$_2$ (4) with I$_2$. In a typical experiment, an ^{1}H NMR spectrum was first recorded for a dry CD_2Cl_2 (0.45 mL) solution of **4** (13 mg). I_2 (1∼2 mg, 0.2−0.4 equiv) was added at room temperature. After being shaken vigorously to dissolve I_2, the solution was monitored by ^{1}H or ^{119}Sn NMR spectroscopy after several minutes. I_2 was added repeatedly to reach a total amount of ∼4 equiv. With I_2 < 1.0 equiv, the products were identified to be a mixture containing MeI (^{1}H, δ = 2.20 ppm), Me$_3$SnI (^{119}Sn, δ = 47.6 ppm), Pt(*N*,*C*,*N*-BAM-)Me(I)(SnMe$_3$) (**10**) (12% yield), Pt(I-BAM)Me$_2$(I)(SnMe$_3$) (**11**) (60% yield), and Pt(*N*,*C*,*N*-BAM)PtMe$_2$(I) (**12a**) (28% yield). Note: The yields of these resulting Pt(IV) species were calculated

Table 1. Crystallographic Data

	1a	**2**	**9·[PtMe$_3$I]$_4$**	**13**	**14**
formula	$C_{18}H_{20}N_4Si$	$C_{20}H_{26}N_4PtSi$	$C_{21}H_{29}N_4I_3Si\ Pt_2$	$C_{17}H_{17}N_4I_3Sn\ Pt$	$C_{16}H_{14}N_4I_4Pt$
FW	320.47	545.63	1136.45	971.83	965.00
space group	*Cmca*	$P\bar{1}$	$P4_2/n$	$Pca2_1$	$P2_1/c$
a, Å	19.2611(13)	9.2748(11)	24.238(3)	18.376(19)	11.063(2)
b, Å	12.5501(8)	9.5207(12)	24.238(3)	8.701(9)	17.067(2)
c, Å	14.3500(9)	13.2059(16)	9.759(3)	14.580(15)	12.6668(17)
α, deg	90	104.3020(10)	90	90	90
β, deg	90	106.3130(10)	90	90	114.524(10)
γ, deg	90	94.5730(10)	90	90	90
V, Å^3	3468.8(4)	1070.5(2)	5733.5(18)	2331(4)	2175.8(6)
Z	8	2	8	4	4
D_{calc}, g·cm^{-3}	1.227	1.693	2.633	2.769	2.946
T, K	298	298	298	180	298
μ, mm^{-1}	0.140	6.621	13.038	11.047	12.132
$2\theta_{max}$, deg	54.26	54.52	56.52	52.00	54.28
reflns measured	18666	12142	64078	22011	5484
reflns used (R_{int})	1981 (0.024)	4671 (0.022)	6925 (0.096)	4556 (0.0570)	3380 (0.024)
parameters	120	250	286	237	222
R [$I > 2\sigma I$]]:					
R_1[a]	0.0374	0.0173	0.0408	0.0272	0.0352
wR_2[b]	0.1016	0.0399	0.0855	0.0567	0.0804
R (all data):					
R_1[a]	0.0446	0.0195	0.0912	0.0354	0.0491
wR_2[b]	0.1086	0.0405	0.1012	0.0602	0.0891
GOF on F^2	1.070	1.027	1.017	0.903	1.074

[a] $R_1 = \Sigma||F_o| - |F_c||/\Sigma|F_o|$. [b] $wR_2 = [\Sigma w\,[(F_o^2 - F_c^2)^2]/\Sigma[w(F_o^2)^2]]^{1/2}$, $w = 1/[\sigma^2(F_o^2) + (0.075P)^2]$, where $P = [\max(F_o^2,0) + 2F_c^2]/3$.

according to the relative integrations of their diagnostic ^{1}H NMR signals against the residual solvent peak; requisite weigh corrections were considered. Diagnostic ^{1}H NMR (500 Hz, CD_2Cl_2, 25 °C) of **10**: δ 8.87 (d, satellites; $^3J = 5.5$ Hz, $^3J_{Pt-H} = 16.1$ Hz; 1H, 7-aza), 8.79 (d, satellites; $^3J = 5.5$ Hz, $^3J_{Pt-H} = 14.0$ Hz; 1H, 7-aza), 6.36 (s, satellites; $^2J_{Pt-H} = 19.0$ Hz; 1H, bridging C*H*) ppm. Diagnostic ^{1}H NMR (500 Hz, CD_2Cl_2, 25 °C) of **11**: δ 8.98 (br; 1H, 7-aza), 8.73 (d; $^3J = 6.5$ Hz; 1H, 7-aza), 6.51 (s; 1H, bridging C*H*), −0.04 (s, satellites; $^2J_{Sn-H} = 49.8$, $^2J_{Pt-H} = 8.1$ Hz; 9H, Pt−Sn*Me*$_3$) ppm. ^{119}Sn NMR of **11**: δ −86.1 ppm (^{195}Pt−^{119}Sn coupling is not resolved because of the insufficient concentration). Diagnostic ^{1}H NMR (500 Hz, CD_2Cl_2, 25 °C) of **12a**: δ 9.21 (d, satellites; $^3J = 7.0$ Hz, $^3J_{Pt-H} = 30.1$ Hz; 1H, 7-aza), 7.06 (s, satellites; $^2J_{Pt-H} = 23.8$ Hz; 1H, bridging C*H*), 2.18 (s, satellites; $^2J_{Pt-H} = 70.5$ Hz; 1H, Pt-Me) ppm. Further addition of excess I_2 (∼4.0 equiv in total) led to a mixture of MeI, Me_3SnI_3 (^{119}Sn, $\delta = 49.3$ ppm), Pt(*N*,*C*,*N*-BAM)Me(SnMeI$_2$)(I) (**13**), Pt(*N*,*C*,*N*-BAM)Me(I)(I$_3$) (**14**), **I-BAM**, and an unresolved Pt^{IV} compound (^{1}H: δ 1.31 (s, satellites; $^2J_{Pt-H} = 65.0$ Hz; 6H, Pt-*Me*), 0.93 (s, satellites; $^2J_{Sn-H} = 56.6$ Hz; 9H, Sn*Me*$_3$)). ^{1}H NMR (400 Hz, CD_2Cl_2, 25 °C) of **I-BAM**: δ 8.85−8.78 (m; 2H, 7-aza), 8.0 (m; 2H, 7-aza), 7.65 (m; 2H, 7-aza), 7.19 (m; 2H, 7-aza), 6.84 (m; 2H, 7-aza), 6.73 (br; bridging C*H*-I) ppm. ^{1}H NMR (400 Hz, CD_2Cl_2, 25 °C) of complex **13**: δ 8.89 (d, satellites; $^3J = 5.6$ Hz, $^3J_{Pt-H} = 12.0$ Hz; 1H, 7-aza), 8.81 (d, satellites; $^3J = 5.2$ Hz, $^3J_{Pt-H} = 10.4$ Hz; 1H, 7-aza), 8.05−7.94 (m; 2H, 7-aza), 7.60−7.55 (m; 2H, 7-aza), 7.18−7.10 (m; 2H, 7-aza), 6.89−6.85 (m; 2H, 7-aza), 6.70 (s, satellites; $^2J_{Pt-H} = 8.0$ Hz; 1H, bridging C*H*), 1.97 (s, satellites; $^2J_{Pt-H} = 55.6$ Hz; 3H, Pt-*Me*), 1.37 (s, satellites; $^2J_{Sn-H} = 7.0$ Hz; 3H, Pt−SnI$_2$*Me*) ppm. ^{1}H NMR (400 Hz, CD_2Cl_2, 25 °C) of complex **14**: δ 9.19 (d, satellites; $^3J = 5.2$ Hz, $^3J_{Pt-H} = 29.6$ Hz; 1H, 7-aza), 8.96 (d, satellites; $^3J = 4.8$ Hz, $^3J_{Pt-H} = 8.8$ Hz; 1H, 7-aza), 8.02−7.95 (m; 2H, 7-aza), 7.64−7.58 (m; 2H, 7-aza), 7.20−7.15 (m; 2H, 7-aza), 7.05 (s, satellites; $^2J_{Pt-H} = 23.6$ Hz; 1H, bridging C*H*), 7.01 (d; $^3J = 3.6$ Hz; 1H, 7-aza), 6.82 (d; $^3J = 3.6$ Hz; 1H, 7-aza), 2.17 (s, satellites; $^2J_{Pt-H} = 70.4$ Hz; 3H, Pt-*Me*) ppm.

Reactivity Study of Pt(*N*,*C*,*N*-BAM)Me$_3$ (M1, Chart 1) with I$_2$. An ^{1}H NMR spectrum was first recorded for a dry CD_2Cl_2 (0.45 mL) solution of complex **M1** (∼5 mg). I_2 (2.5 mg, ∼1 equiv) was then added at room temperature. After being shaken vigorously to dissolve I_2, the resulting light yellow solution was monitored by ^{1}H NMR spectroscopy after several minutes, and the products generated were identified to be a mixture containing MeI (^{1}H, δ = 2.20 ppm) and complex Pt(*N*,*C*,*N*-BAM)PtMe$_2$(I) (**12b**), which is a geometrical isomer of **12a**. ^{1}H NMR (400 Hz, CD_2Cl_2, 25 °C) of **12b**: δ 8.93 (d, satellites; $^3J = 4.8$ Hz,$^4J = 1.0$ Hz,$^3J_{Pt-H} = 9.2$ Hz; 2H, 7-aza), 7.97 (dd; $^3J = 7.8$ Hz, $^4J = 1.0$ Hz; 2H, 7-aza), 7.60 (d; $^3J = 3.6$ Hz; 2H, 7-aza), 7.16 (dd; $^3J_1 = 4.8$ Hz, $^3J_2 = 4.8$ Hz; 2H, 7-aza), 6.80 (d; $^3J = 3.6$ Hz; 2H, 7-aza), 6.39 (s, satellites; $^2J_{Pt-H} = 19.3$ Hz; 1H, bridging C*H*), 1.34 (s, satellites; $^2J_{Pt-H} = 71.3$ Hz; 6H, Pt*Me*$_2$) ppm. Further addition of excess I_2 (3 equiv) did not result in obvious ^{1}H NMR spectral change. Slow evaporation of the CD_2Cl_2 solution afforded red crystals, which were characterized by single-crystal X-ray diffraction analyses to be complex Pt(*N*,*C*,*N*-BAM)PtMe$_2$(I$_3$) (**15**). The X-ray data for complex **15** are provided in the Supporting Information. Anal. Calcd for complex **15**, $C_{17}H_{17}N_4I_3Pt$: C, 23.93; H, 2.01; N, 6.57. Found: C, 24.23; H, 2.06; N, 6.54.

X-ray Diffraction Analyses. Single crystals of Me$_3$Si-BAM (ligand **1a**), **2**, **7**, **9·[PtMe$_3$I]$_4$**, **9·I$_2$**, and **13**−**15** were mounted on glass fibers for data collection. Data were collected on a Bruker Apex II single-crystal X-ray diffractometer with graphite-monochromated Mo Kα radiation, operating at 50 kV and 30 mA. No significant decay was observed in any samples. Data were processed on a PC with the aid of the Bruker SHELXTL software package (version 5.10) and corrected for absorption effects. All structures were solved by direct methods. Most of the non-hydrogen atoms were refined anisotropically. The positions of hydrogen atoms were calculated, and their contributions in structural factor calculations were included. The crystal structure of **7** shows severe disordering and twining, and as a result, the quality of the structure data is poor despite our best efforts. The crystal of **14** belongs to the monoclinic space group $P2_1/c$, but its data were collected as an orthorhombic crystal system due to the improper determination of the initial unit cell parameters, resulting in ∼72% of the unique data collected for **14**, and because of it, not all non-hydrogen atoms can be refined anisotropically. Nonetheless, the data allow us to establish the basic structural features of **14** unambiguously. The crystal data of **1a**, **2**, **9·[PtMe$_3$I]$_4$**, **13**, and **14** are given in Table 1. Important bond lengths and angles for all the compounds are listed in Table 2. Data for other structures are shown in the Supporting Information.

Table 2. Selected Bond Lengths (Å) and Angles (deg)

	Compound **1a**		
Si(1)−C(10)	1.8486(18)	C(9)−Si(1)−C(1)	113.29(13)
Si(1)−C(9)	1.858(3)	C(8)−N(1)−C(2)	107.40(11)
Si(1)−C(1)	1.9131(19)	C(8)−N(1)−C(1)	124.67(11)
N(1)−C(8)	1.3746(16)	C(2)−N(1)−C(1)	127.19(12)
N(1)−C(2)	1.3843(17)	C(8)−N(2)−C(7)	113.81(13)
N(1)−C(1)	1.4639(14)	N(1)−C(1)−Si(1)	114.16(8)
	Compound **2**		
Pt(1)−C(1)	2.031(3)	Si(1)−C(10)	1.902(3)
Pt(1)−C(2)	2.037(3)	C(1)−Pt(1)−C(2)	89.12(14)
Pt(1)−N(1)	2.135(2)	C(1)−Pt(1)−N(1)	177.67(10)
Pt(1)−N(4)	2.142(2)	C(2)−Pt(1)−N(1)	90.50(12)
Si(1)−C(19)	1.849(3)	C(1)−Pt(1)−N(4)	89.07(11)
Si(1)−C(18)	1.856(3)	C(2)−Pt(1)−N(4)	178.15(12)
Si(1)−C(20)	1.874(3)	N(1)−Pt(1)−N(4)	91.32(8)
	Compound **9**·$[PtMe_3I]_4$		
Pt(1)−N(4)	2.048(6)	N(1)−Pt(1)−I(2)	89.92(19)
Pt(1)−N(1)	2.056(7)	N(4)−Pt(1)−I(1)	88.27(19)
Pt(1)−I(2)	2.5831(8)	N(1)−Pt(1)−I(1)	178.1(2)
Pt(1)−I(1)	2.5833(7)	I(2)−Pt(1)−I(1)	91.95(3)
Pt(2)−C(20)	2.069(11)	C(20)−Pt(2)−C(21)	90.6(5)
Pt(2)−C(21)	2.092(11)	C(20)−Pt(2)−C(19)	89.6(6)
Pt(2)−C(19)	2.108(11)	C(21)−Pt(2)−C(19)	89.1(6)
Pt(2)−I(3)	2.8066(9)	C(20)−Pt(2)−I(3)	90.4(4)
N(4)−Pt(1)−N(1)	89.9(3)	C(21)−Pt(2)−I(3)	177.9(4)
N(4)−Pt(1)−I(2)	175.78(19)	C(19)−Pt(2)−I(3)	92.7(5)
	Compound **13**		
Sn(1)−C(17)	2.179(8)	C(15)−Pt(1)−C(16)	91.4(3)
Sn(1)−Pt(1)	2.547(2)	C(15)−Pt(1)−N(1)	88.9(3)
Sn(1)−I(3)	2.731(2)	C(16)−Pt(1)−N(1)	83.2(3)
Sn(1)−I(2)	2.738(2)	C(15)−Pt(1)−N(3)	173.4(3)
Pt(1)−C(15)	2.083(8)	C(16)−Pt(1)−N(3)	82.3(3)
Pt(1)−C(16)	2.094(8)	N(1)−Pt(1)−N(3)	92.3(3)
Pt(1)−N(1)	2.160(7)	C(15)−Pt(1)−Sn(1)	86.1(3)
Pt(1)−N(3)	2.176(7)	C(16)−Pt(1)−Sn(1)	94.6(2)
Pt(1)−I(1)	2.699(2)	N(1)−Pt(1)−Sn(1)	174.42(18)
C(17)−Sn(1)−Pt(1)	123.9(3)	N(3)−Pt(1)−Sn(1)	92.47(18)
C(17)−Sn(1)−I(3)	102.4(2)	C(15)−Pt(1)−I(1)	91.3(3)
Pt(1)−Sn(1)−I(3)	112.63(5)	C(16)−Pt(1)−I(1)	177.3(2)
C(17)−Sn(1)−I(2)	101.8(3)	N(1)−Pt(1)−I(1)	96.6(2)
Pt(1)−Sn(1)−I(2)	110.21(5)	N(3)−Pt(1)−I(1)	95.0(2)
I(3)−Sn(1)−I(2)	103.72(8)	Sn(1)−Pt(1)−I(1)	85.86(5)
	Compound **14**		
Pt(1)−C(16)	2.043(11)	C(15)−Pt(1)−N(1)	171.8(4)
Pt(1)−N(3)	2.086(8)	C(16)−Pt(1)−I(1)	90.9(3)
Pt(1)−C(15)	2.146(8)	N(3)−Pt(1)−I(1)	174.3(3)
Pt(1)−N(1)	2.177(8)	C(15)−Pt(1)−I(1)	91.2(2)
Pt(1)−I(1)	2.6049(9)	N(1)−Pt(1)−I(1)	88.3(2)
Pt(1)−I(2)	2.7106(10)	C(16)−Pt(1)−I(2)	178.0(3)
I(2)−I(3)	3.0669(11)	N(3)−Pt(1)−I(2)	95.7(3)
I(3)−I(4)	2.7889(12)	C(15)−Pt(1)−I(2)	92.7(3)
C(16)−Pt(1)−N(3)	83.4(4)	N(1)−Pt(1)−I(2)	95.5(2)
C(16)−Pt(1)−C(15)	89.0(4)	I(1)−Pt(1)−I(2)	89.94(3)
N(3)−Pt(1)−C(15)	88.1(3)	Pt(1)−I(2)−I(3)	105.68(3)
C(16)−Pt(1)−N(1)	82.7(4)	I(4)−I(3)−I(2)	178.57(4)
N(3)−Pt(1)−N(1)	91.7(3)		

Results and Discussion

Syntheses and Characterization of Ligands 1a−1c and Their Reactions with PtR_2 (R = Me, Ph). Ligand Synthesis. Treatment of in situ generated bis(7-azaindol-1-yl)methyllithium salt with electrophiles Me_3SiCl and R_3SnCl (R = Me, Ph) in dry THF at −78 °C afforded the BAM derivative ligands $SiMe_3$-BAM (**1a**), $SnMe_3$-BAM (**1b**), and $SnPh_3$-BAM (**1c**), respectively, with 55−72% isolated yield after aqueous workup (Scheme 1). Compounds **1a**−**c** have been fully characterized by NMR and HRMS analyses. The structure of **1a** has also been verified by X-ray diffraction analysis (Figure 1).

Scheme 1

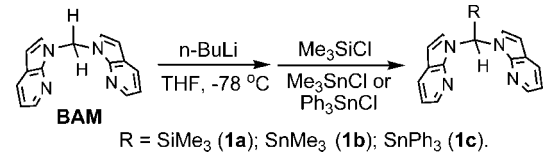

Scheme 2[a]

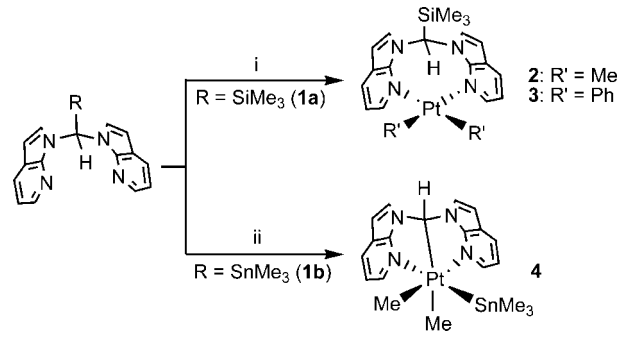

[a] Reaction conditions: (i) $[PtMe_2(\mu\text{-}SMe_2)]_2$ or $[PtPh_2(\mu\text{-}SMe_2)]_n$ (n = 2, 3), THF, rt, overnight; (ii) $[PtMe_2(\mu\text{-}SMe_2)]_2$, CH_2Cl_2, rt, overnight.

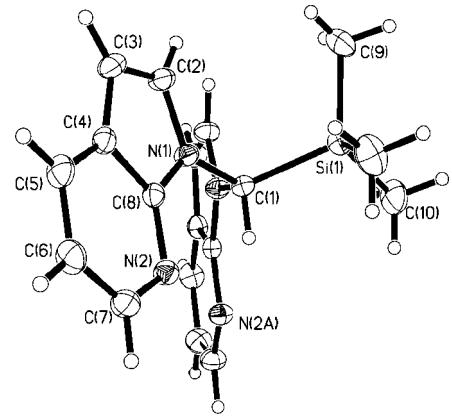

Figure 1. Crystal structure of **1a**.

Reactions of $SiMe_3$-BAM (1a) with $Pt^{II}R_2$ (R = Me, Ph). Ligand displacement reactions of **1a** with $[PtMe_2(\mu\text{-}SMe_2)]_2$ and $[PtPh_2(\mu\text{-}SMe_2)]_n$ (n = 2, 3) generated the *N*,*N*-chelating Pt(II) complexes **2** and **3** (Scheme 2), respectively, as colorless crystalline solids, which have been fully characterized. The structure of **2** determined by X-ray diffraction analysis is shown in Figure 2. The Pt(II) center in **2** has a typical square planar geometry, with the $SiMe_3$ group oriented away from the $PtMe_2$ moiety. The $Pt\cdots H{-}C_{BAM}$ separation distance (∼2.24 Å) in **2** is much shorter than that (∼2.44 Å) in complex $Pt(BAM)Me_2$,[3] an indication of a stronger three-center four-electron $Pt^{II}\cdots H{-}C$ electrostatic interaction[5] in **2**. Similar to previous BAM Pt^{II} complexes,[3,5] both **2** and **3** display a diagnostic low-field ^1H resonance for their bridging methine groups due to such three-center four-electron $Pt^{II}\cdots H{-}C$ interactions,[5] with δ = 13.13 and 12.60 ppm, respectively. This signal is further characterized by the distinct $^{195}Pt{-}^1H$ coupling satellites, with J_{Pt-H} = 61.0 and 44.1 Hz for **2** and **3**, respectively. Compounds **2** and **3** display a good thermal stability since heating them in C_6D_6 at 75 °C over several days did not result in obvious changes in their ^1H NMR spectra.

Reactions of $SnMe_3$-BAM (1b) with PtR_2 (R = Me, Ph). With $[PtMe_2(SMe_2)]_2$. The $SnMe_3$ derivative **1b** exhibited a markedly different reaction pattern when reacted with the two

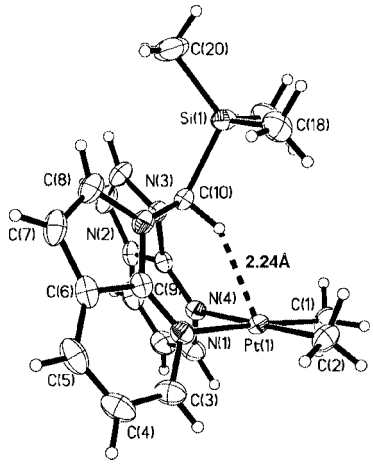

Figure 2. Crystal structure of complex **2**.

Pt(II) precursors. As shown in Scheme 2, its reaction with $[PtMe_2(\mu\text{-}SMe_2)]_2$ produced cleanly a neutral six-coordinate Pt(IV) complex Pt(*N*,*C*,*N*-BAM)Me$_2$(SnMe$_3$) (**4**), in which the Me$_3$Sn−C$_{BAM}$ bond has been broken and *cis* oxidatively added to the Pt center, instead of the *N*,*N*-chelating complex Pt(Me$_3$Sn-BAM)Me$_2$. In **4**, the BAM ligand adopts a similar κ^3-N,C,N chelating mode as observed in complex **M1** (Chart 1).[11] Complex **4** is an air- and moisture-stable oil at room temperature and fully characterized by NMR as well as HRMS. The complete ^{1}H NMR spectrum of **4** along with the assignments of the most diagnostic ^{1}H signals is shown in Figure 3. The CH group in **4** exhibits a ^{1}H resonance at 5.95 ppm with distinct ^{195}Pt−^{1}H coupling satellites ($^2J_{Pt-H}$ = 26.0 Hz), characteristic of κ^3-N,C,N BAM-bonded Pt(IV) species,[11] thus indicating the formation of a Pt−C$_{BAM}$ bond. Moreover, the SnMe$_3$ group displays an upfield-shifted ^{1}H resonance at −0.22 ppm (0.26 ppm in **1b**), with distinct satellites from both ^{195}Pt ($^3J_{Pt-H}$ = 10.5 Hz) and $^{117/119}$Sn ($^2J_{Sn-H}$ = 47.5 Hz) couplings, thus supporting the formation of a Pt−SnMe$_3$ bond in **4**. Furthermore, the observation of two sets of distinct Pt-*Me* and 7-azaindolyl signals suggests the lack of symmetry in **4**, thus the occupation of the basal position by the SnMe$_3$ group. Additionally, in the ^{119}Sn spectrum ligand **1b** displays a singlet at −7.3 ppm, but complex **4** has a high-field ^{119}Sn resonance (δ = −84.4 ppm) with diagnostic ^{195}Pt coupling satellites ($^2J_{Pt-Sn}$ = 10728.7 Hz)[14] (see Figure S7 in the Supporting Information), hence providing further compelling spectroscopic evidence for the formation of a Pt−Sn bond in **4**.

Although oxidative addition of Sn(IV) halides to electron-rich Pt(II) centers is a well-established phenomenon,[14] tetraalkyltin compounds are usually not reactive under similar conditions due to the low electrophilicity of their Sn−C bonds. To gain insight into the unusual generation of **4**, the reaction of **1b** with $[PtMe_2(\mu\text{-}SEt_2)]_2$ (1 equiv) in CD_2Cl_2 ([**1b**] ∼0.03 M) was monitored using ^{1}H NMR spectroscopy. The resulting ^{1}H NMR spectra are shown in Figure 4, with the product distribution plot shown in Figure 5. Noteworthy is the formation of the N,N-chelating complex Pt(Me$_3$Sn-BAM)Me$_2$ in the early stage of the reaction, as evidenced by the evolution of a diagnostic peak at 12.82 ppm with both ^{195}Pt and ^{117,119}Sn coupling patterns, accompanied by the concomitant formation of **4**. As demonstrated by Figure 5, the N,N-chelating PtMe$_2$ complex was found to transform gradually to complex **4** over time, suggesting that the formation of the N,N-chelating Pt(II) complex is a kinetically favored process whereas the N,C,N-chelating Pt(IV) complex is thermodynamically preferred.

With [PtPh$_2$(SMe$_2$)]$_n$. The reaction of **1b** with $[PtPh_2(\mu\text{-}SMe_2)]_n$ (n = 2, 3) is much slower and affords a mixture consisting of Pt(Me$_3$Sn-BAM)Ph$_2$ (**5**) and Pt(*N*,*C*,*N*-BAM)Ph$_2$(SnMe$_3$) (**6**) (Scheme 3), both of which were characterized by NMR. NMR experiments revealed that **5** is the dominant species at the early stage of the reaction, and it converts slowly into **6** during the course of a few weeks at room temperature (see Figure S9 in the Supporting Information). This is in good agreement with the thermodynamic preference for the *N*,*C*,*N*-chelating Pt(IV) complex other than the *N*,*N*-chelating Pt(II) complex that is kinetically favored.

Possible Reaction Pathway for the Formation of 4 and 6. It is well recognized that stepwise S$_N$2 oxidative additions involving Pt(II) centers usually occur for highly polarized C−I or Sn−X (X = halide) bonds and result in C−I or Sn−X *trans* addition adducts. Therefore, the *cis* configurations of **4** and **6** strongly support a concerted oxidative addition pathway that requires the intermediacy of a σ-Sn−C$_{BAM}$ bonded Pt(II) species. A possible reaction pathway is shown in Scheme 4, where the initial ligand displacement of **1b** with $[PtR_2(\mu\text{-}SMe_2)]_n$ (R = Me, Ph) affords an η^1-*N*-(Me$_3$Sn-BAM)-bonded PtR$_2$(SMe$_2$) intermediate **A**. Subsequent dissociation of SMe$_2$ can either result in the N,N-chelating PtR$_2$ complex or enable a C−Sn oxidative addition process, via a σ-C$_{BAM}$−Sn-bonded Pt(II) intermediate **B** and a five-coordinate Pt(IV) intermediate **C**, that eventually leads to complex **4** or **6**, which may also be obtained directly from the N,N-chelate Pt(II) complex.

Reactions of SnPh$_3$-BAM (1c) with PtR$_2$ (R = Me, Ph). Compound **1c** reacted with $[PtPh_2(\mu\text{-}SMe_2)]_n$ (n = 2, 3) resulting in the N,N-chelating Pt(Ph$_3$Sn-BAM)Ph$_2$ (**7**) in 77% yield (Scheme 5). However, its reaction with $[PtMe_2(\mu\text{-}SMe_2)]_2$ was surprisingly complicated. As revealed by ^{1}H NMR experiments, multiproducts were formed even in the early stage of the reaction, and a stable mixture was achieved in about 10 h (see Figure S11 in the Supporting Information). Despite difficulties in resolving all of the final products, four diagnostic ^{1}H signals in the region of 12.5−13.8 ppm can be attributed to N,N-chelating Pt^{II} species, while three diagnostic ^{1}H signals in the region of 5.8 to 6.1 ppm can be attributed to N,C,N-chelating BAM Pt^{IV} species. The major product was identified unexpectedly to be complex **7** according to various NMR evidence (Scheme 5). The identity of **7** was further confirmed by X-ray diffraction analysis despite the poor quality of the data (see the Supporting Information). These findings suggest the involvement of an intermolecular Sn^{IV}-*Ph* and Pt^{II}-*Me* metathesis process for the reaction of **1c** with $[PtMe_2(\mu\text{-}SMe_2)]_2$.

Possible Reaction Pathway for the Formation of 7. The transfer of aryl groups from organotins to Pd^{II} centers serves as a crucial step in Pd-mediated Stille-type C−C coupling processes.[15] In contrast, analogous processes on Pt^{II} centers are rather rare, albeit not unknown, as illustrated by the synthesis of *cis*-Pt(DMSO)$_2$Ph$_2$ via metathesis between PhSnMe$_3$ and Pt(DMSO)$_2$Cl$_2$.[16] Another intriguing example is the recent application of similar processes toward generating organometallic Ir(III) complexes, demonstrated by Bergman et al.[17]

(14) (a) Janzen, M. C.; Jennings, M. C.; Puddephatt, R. J. *Organometallics* **2001**, *20*, 4100. (b) Levy, C. J.; Puddephatt, R. J. *J. Am. Chem. Soc.* **1997**, *119*, 10127. (c) Levy, C. J.; Vittal, J. J.; Puddephatt, R. J. *Organometallics* **1996**, *15*, 2108. (d) Levy, C. J.; Vittal, J. J.; Puddephatt, R. J. *Organometallics* **1996**, *15*, 35. (e) Levy, C. J.; Puddephatt, R. J.; Vittal, J. J. *Organometallics* **1994**, *13*, 1559.

(15) For reviews on the Stille coupling, see: (a) Espinet, P.; Echavarren, A. M. *Angew. Chem., Int. Ed.* **2004**, *43*, 4704. (b) Stille, J. K. *Angew. Chem., Int. Ed.* **1986**, *25*, 508.

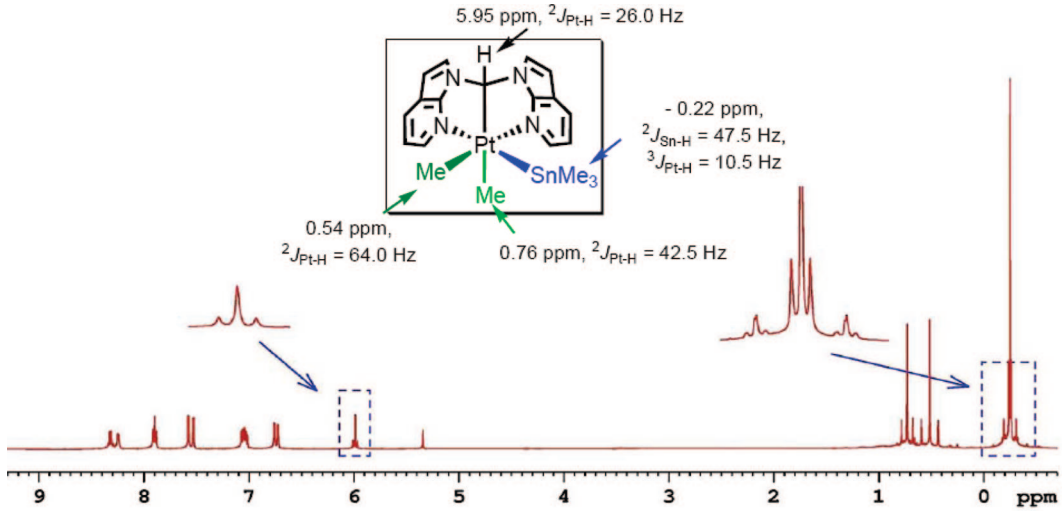

Figure 3. ^{1}H NMR of **4** in CD_2Cl_2 at room temperature.

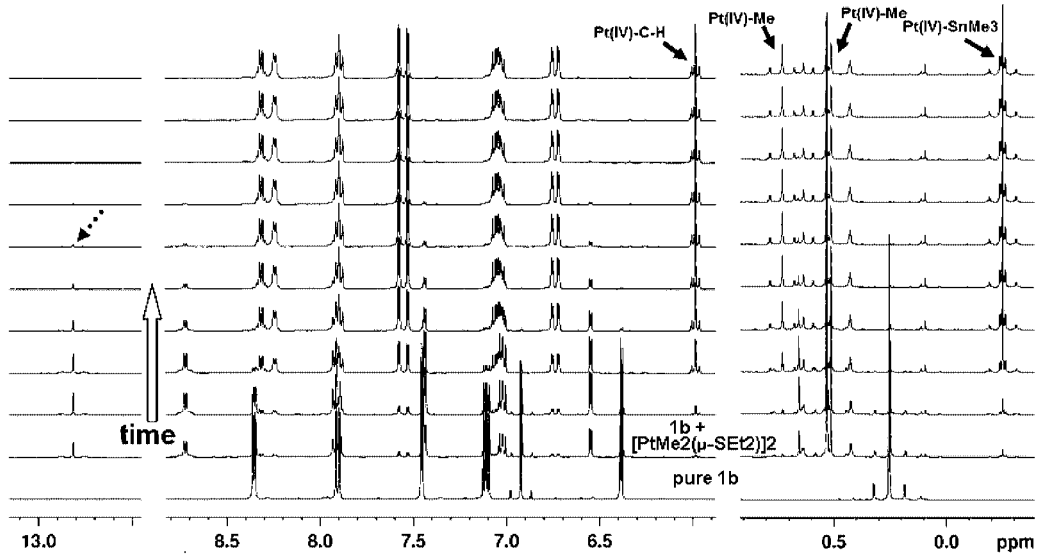

Figure 4. Stacked ^{1}H NMR spectra for the reaction of **1b** with $[PtMe_2(\mu\text{-}SEt_2)]_2$ in CD_2Cl_2 at room temperature.

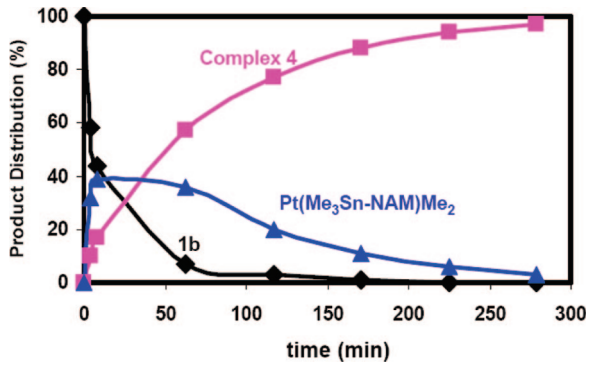

Figure 5. Product distribution plot for the reaction of **1b** with $[PtMe_2(\mu\text{-}SEt_2)]_2$.

To better understand the unexpected formation of complex **7**, we carried out several control experiments. We have found that Pt(BAM)Me_2 and $[PtMe_2(\mu\text{-}SEt_2)]_2$ both undergo slow Pt^{II}-*Me*/Sn^{IV}-*Ph* metathesis with Ph_4Sn (1 equiv) at room temperature in CD_2Cl_2, with 40−60% conversion achieved after 3 days (see Figure S12, Supporting Information), thus indicating the feasibility for a direct Sn^{IV}-*Ph* and Pt^{II}-*Me* metathesis process

Scheme 3

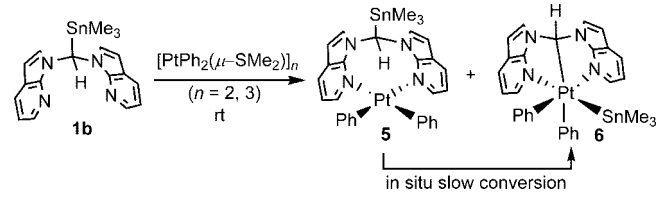

for the reaction of **1c** with $[PtMe_2(\mu\text{-}SMe_2)]_2$ under the conditions used. Furthermore, despite containing a Ph_3Sn moiety, complex **7** was found not reactive with $[PtMe_2(\mu\text{-}SMe_2)]_2$ during the course of three days monitoring, indicating that the coordination of Ph_3Sn-BAM to $PtPh_2$ reduces its reactivity, perhaps due to the increased steric congestion around the Sn^{IV} center. On the basis of these facts as well as previous knowledge, a Sn^{IV}−Ph and Pt^{II}−Me metathesis pathway for the formation of complex **7** is proposed and shown in Scheme 6. The reaction

(16) (a) Romeo, R.; Monsù Scolaro, L. *Inorg. Synth.* **1998**, *32*, 153. (b) Eaborn, C.; Kundu, K.; Pidcock, A. *J. Chem. Soc., Dalton Trans.* **1981**, 933.

(17) Smith, S. E.; Sasaki, J. M.; Bergman, R. G.; Mondloch, J. E.; Finke, R. G. *J. Am. Chem. Soc.* **2008**, *130*, 1839.

Scheme 4

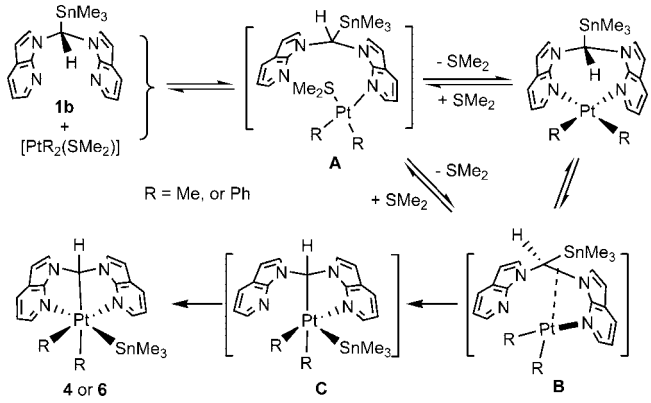

Scheme 5

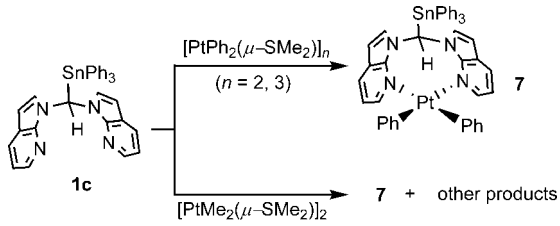

Scheme 6. Proposed Sn^{IV}-*Ph* and Pt^{II}-*Me* Metathesis Process between 1c and [PtMe$_2$(*μ*-SMe$_2$)]$_2$

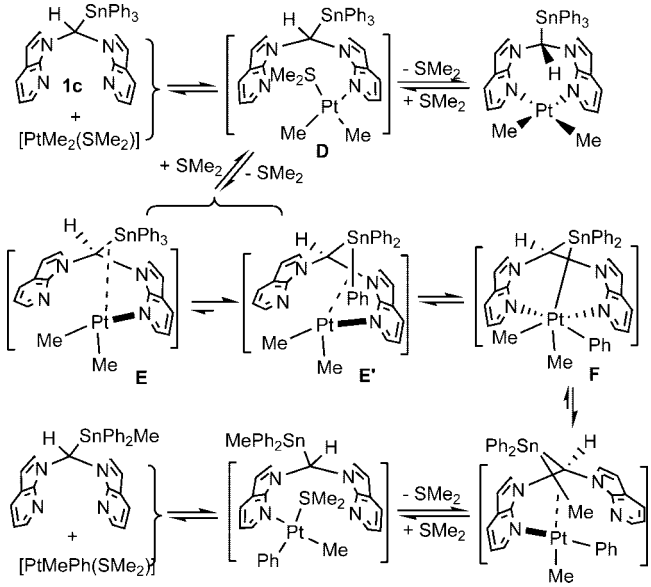

of **1c** with [PtMe$_2$(*μ*-SMe$_2$)]$_2$ would afford initially a η^1-*N*-Ph$_3$Sn-BAM-bonded PtMe$_2$(SMe$_2$) species (**D**). Subsequent dissociation of SMe$_2$ results in the N,N-chelating PtMe$_2$ complex, which may have even higher instability compared to its Me$_3$Sn analogue because of the large size of Ph$_3$Sn. Dissociation of SMe$_2$ from **D** can lead to a σ-C$_{BAM}$−Sn-bonded intermediate **E** and a σ-Sn−Ph-bonded Pt(II) intermediate **E′**. Due to the large size of SnPh$_3$ compared to SnMe$_3$, the formation of **E′** other than **E** is likely energetically favored. Subsequent Sn-Ph *cis* oxidative addition from **E′** results in a k^3-N,Sn,N-bonded Pt^{IV} complex **F**. However, **F** is highly strained, and the two six-membered Pt−Sn−C−N−C−N metallocycles are disfavored compared to the two five-membered Pt−C−N−C−N metallocycles in complex **4** or complex **M1**,[11] which may enable an irreversible Sn^{IV}−CH$_3$ reductive coupling, thus completing a single Sn^{IV}-*Ph* and Pt^{II}-*Me* exchange process. The resulting new ligand could undergo a similar process through intermediates analogous to **E′**, resulting in further Sn^{IV}-*Ph* and Pt^{II}-*Me* exchange, and eventually generating [PtPh$_2$(*μ*-SMe$_2$)]$_n$ (n = 2, 3), which can bind with **1c** to produce **7**.

It should be noted that transition-metal complexes with a similar k^3-*N*,*Sn*,*N*-chelating mode such as **F** are not unprecedented. In fact, treatments of ^{t}Bu$_2$PhSn-CH(Pz′)$_2$ (Pz′ = 3,5-dimethylpyrazol-1-yl, or 3,4,5-trimethylpyrazol-1-yl) with W(CO)$_5$(THF) were demonstrated previously to give rise to two stable k^3-N,Sn,N-chelating W(II) products, in which the ligand Sn-*Ph* bond is selectively and oxidatively added to the W center.[12i] Besides the two starting materials, similar Sn^{IV}-*Ph* and Pt^{II}-*Me* metathesis processes could theoretically result in not only Pt^{II} species such as [PtMePh(SMe$_2$)] and [PtPh$_2$(SMe$_2$)] but also new ligands Ph$_2$MeSn-BAM, PhMe$_2$Sn-BAM, and **1b**, which can of course react with Pt(II) and lead to the generation of multiple products from the reaction of [PtMe$_2$(*μ*-SMe$_2$)]$_2$ with **1c**.

Reactivity of Pt(SiMe$_3$-BAM)Me$_2$ (2), Pt(*N*,*C*,*N*-BAM)-(SnMe$_3$)Me$_2$ (4), and Pt(*N*,*C*,*N*-BAM)Me$_3$ (M1). Reactivity of 2 with MeI and MeOTf. The reactivity of **2** toward MeI and MeOTf was examined to understand the steric impact of the Me$_3$Si group on the formation of *fac*-Pt^{IV}Me$_3$ complexes. The behavior of **2** was found to be similar to Pt(BAM)Me$_2$.[11] NMR experiments revealed that **2** reacts spontaneously with MeI at room temperature, giving rise to free ligand **1a** and the tetrameric complex [PtMe$_3$I]$_4$, illustrating the poor stability of **1a** when competing with I$^-$ for binding the Pt^{IV}Me$_3$ cation.[11] The addition of MeOTf to a CD$_2$Cl$_2$ solution of **2** converted it quantitatively to a five-coordinate Pt^{IV}Me$_3$ complex [Pt(Me$_3$Si-BAM)Me$_3$][OTf] (**8**), characterized by NMR spectra (Figure 6), where the methine proton peak shifts from 13.13 ppm in **2** to 5.00 ppm in **8**, attributable to the change of a "three-center four-electron" Pt···H−C$_{BAM}$ interaction[5] in **2** to a "three-center two-electron" interaction in **8**.[11] Consistent with the Pt^{II} → Pt^{IV} oxidation state change is the δ downfield shift (0.67 ppm → 1.79 ppm) of the Pt-*Me* signal (Figure 6). Compound **8** only displays one well-defined Pt-*Me* peak, indicating the presence of a rapid methyl exchange process, as found in other Pt^{IV}Me$_3$ species.[8,9,11] In contrast to the previously reported BAM *fac*-Pt^{IV}Me$_3$ complexes that have a good stability, **8** is unstable in solution at room temperature and slowly degrades, giving rise to the tetrameric complex [PtMe$_3$(OTf)]$_4$ via releasing ligand **1a**. This finding also accounts for our unsuccessful attempts in synthesizing **8** by reacting [PtMe$_3$(OTf)]$_4$ with ligand **1a**. The instability of **8** can be attributed to the steric repulsion induced by the bulky SiMe$_3$ moiety.

Reactivity of 2 with I$_2$. Considerable recent efforts have been taken in the study of competing C−C and C−X (X = halogen atoms) reductive elimination processes by examining (N,N)Pt^{IV}R$_2$(I)$_2$ complexes (R = alkyl, aryl),[18] which can be prepared most conveniently by S$_N$2 oxidative addition reactions of I$_2$ to the corresponding (N,N)Pt^{II}R$_2$ complexes. In contrast, complex **2** showed different behaviors when its iodinolysis was attempted for the synthesis of Pt^{IV}(SiMe$_3$-BAM)Me$_2$(I)$_2$. Treatment of **2** with 1 equiv of I$_2$ in CD$_2$Cl$_2$ resulted in several species, identified as Pt(Me$_3$Si-BAM)(I)$_2$ (**9**), MeI, [PtMe$_3$I]$_4$,[19] and ligand **1a**, respectively (see S13 in the Supporting Information). Compound **9** and [PtMe$_3$I]$_4$ co-crystallized in a 4:1 ratio

(18) (a) Yahav-Levi, A.; Goldberg, I.; Vigalok, A.; Vedernikov, A. N. *J. Am. Chem. Soc.* **2008**, *130*, 724. (b) Yahav-Levi, A.; Goldberg, I.; Vigalok, A. *J. Am. Chem. Soc.* **2006**, *128*, 8710. (c) Goldberg, K. I.; Yan, J.; Breitung, E. M. *J. Am. Chem. Soc.* **1995**, *117*, 6889.

(19) (a) Clegg, D. E.; Hall, J. R. *Inorg. Synth.* **1967**, *10*, 71. (b) Baldwin, J. C.; Kaska, W. C. *Inrog. Chem.* **1975**, *14*, 2020.

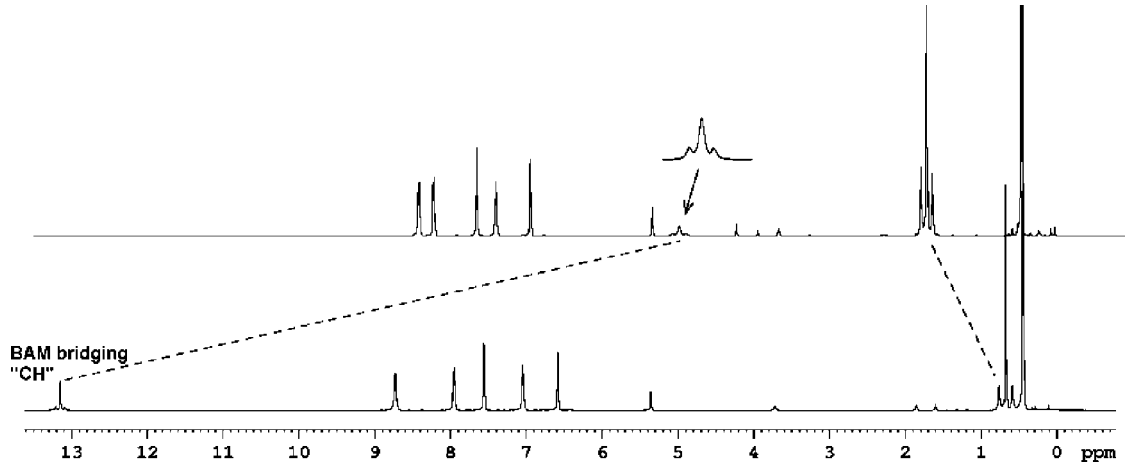

Figure 6. ^{1}H NMR spectra for the conversion of **2** (bottom) to **8** (top) upon addition of MeOTf in CD_2Cl_2 at room temperature.

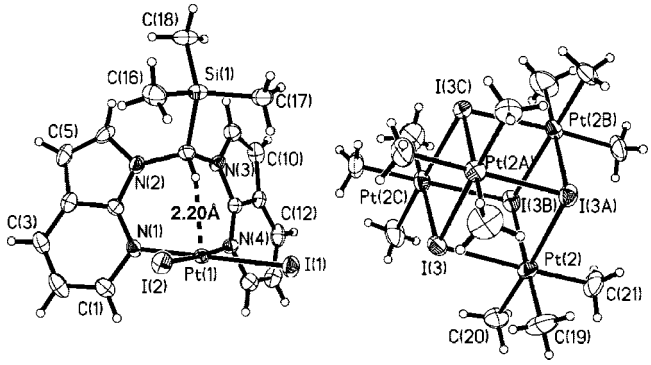

Figure 7. Diagrams showing the structures of **9** and co-crystallized $[PtMe_3I]_4$ with 50% ellipsoids.

upon evaporation of the solvent, and their structures were studied by X-ray diffraction analysis and shown in Figure 7. The structure of **9** resembles that of **2**, with a Pt···*H*−C_{BAM} separation distance of ∼2.20 Å. The mean Pt−I bond length in **9** is 2.5831(8) Å, which is considerably shorter than that (2.8069(9) Å) in the tetrameric complex $[PtMe_3I]_4$, where the mean Pt−Me bond length is 2.096(12) Å.[19,20] Increasing the amount of I_2 to 3 equiv gave rise to a similar mixture that yielded deep red crystals which were characterized by X-ray diffraction analysis to be **9** co-crystallized with I_2 and CH_2Cl_2 (see Supporting Information).

Reaction Mechanism of 2 with I_2. The reaction of **2** with I_2 can be considered as a stoichiometric Pt^{II}-*Me* functionalization process with MeI as the functionalized product. Notably, only a few $Pt^{II}Me_2$ complexes have been reported to produce MeI under mild conditions.[21] A possible reaction mechanism of **2** with I_2 is shown in Scheme 7, where the initial S_N2 oxidative addition of I_2 to **2** generates intermediate **G**. The steric blocking of the Pt(IV) vacant coordination site in **G** prevents the formation of the six-coordinate $Pt^{IV}Me_2(I)_2$ adduct, thus enabling the MeI elimination via nucleophilic attack of Pt^{II}-*Me* by I^-, leading to the formation of an NMR identifiable $Pt^{II}(Me)(I)$ complex, which further reacts with I_2 via a similar process, producing a Pt^{IV} intermediate **H**, and the subsequent formation of **9** and another MeI molecule. As MeI can react very quickly with **2**, the MeI produced competes with I_2 to react with **2**, forming Pt^{IV} intermediate **J** that dissociates to $[PtMe_3I]_4$ and free **1a**. The contrasting behaviors of the Pt^{IV} intermediates **G** and **H** compared to **J** are presumably caused by the different electronic properties of the Pt^{IV} centers. The relative electron-deficient Pt^{IV} centers in **G** and **H** can promote the formation of MeI, whereas the electron-rich Pt^{IV} center in **J** likely favors the ligand dissociation to a greater degree.

Reactivity of 4 with I_2. Making and breaking M−C/Sn bonds represent crucial steps in transition-metal-mediated stoichiometric or catalytic transformation processes;[1,16] thus, the reactivity of the Pt^{IV} complex Pt(*N*,*C*,*N*-BAM)$Me_2(SnMe_3)$ (**4**) was studied. While **4** is not reactive either with $[H(Et_2O)_2]BAr^F{}_4$ (Ar^F = 3,5-bis(trifluoromethyl)phenyl)[22] or $[Bu_4N]I$, it reacts readily with I_2. To detect and identify various species/intermediates involved, the reaction of **4** with I_2 was examined by ^{1}H and ^{119}Sn NMR spectroscopy in dry CD_2Cl_2 (see Figures S14 and S15, Supporting Information). The NMR data showed that with less than 1.0 eq. I_2, the reaction occurred within minutes, producing CH_3I, Me_3SnI, [Pt^{IV}(*N*,*C*,*N*-BAM)Me(I)($SnMe_3$)] (**10**), [Pt^{IV}(*N*,*C*,*N*-BAM)$PtMe_2$(I)] (**12a**), and possibly [Pt^{IV}(I-BAM)Me_2(I)($SnMe_3$)] (**11**) (Scheme 8). The structures of **10** and **12a** were established by NMR data (see Figures S14−S17, Supporting Information), but the structure of **11** could not be fully established using NMR data. According to the integrations of their diagnostic ^{1}H NMR signals against the residual solvent peak, the yields of **10**, **11**, and **12a** are 12%, 60%, and 28%, respectively. Further addition of I_2 (∼4 equiv total) resulted in further NMR spectral change of the mixture, and the final products were identified to be CH_3I, $Me_3Sn(I_3)$, [Pt^{IV}(*N*,*C*,*N*-BAM)Me($SnMeI_2$)(I)] (**13**), [Pt^{IV}(*N*,*C*,*N*-BAM)Me(I)(I_3)] (**14**), I-BAM, and an unresolved Pt^{IV} compound (Scheme 8), according to NMR evidence. The structures of **13** and **14** were confirmed by X-ray diffraction analyses and shown in Figures 8 and 9, respectively, which also validate the proposed structures of **10** and **12a** based on NMR data.

In both **13** and **14**, the BAM ligand adopts a *N*,*C*,*N*-tridentate mode with the Pt(IV) center being six-coordinate, similar to that observed in Pt(*N*,*C*,*N*-BAM)Me_3 (**M1**, Chart 1).[11] In **13**, an I^- resides in the axial position, with a $-Sn(I)_2Me$ group on the basal position cis to the Me group. In **14**, an I_3^- anion occupies the axial position *trans* to the BAM bridging methine group, while an I^- occupies one basal position *cis* to the

(20) Schlecht, S.; Magull, J.; Fenske, D.; Dehnicke, K. *Angew. Chem., Int. Ed. Engl.* **1997**, *36*, 1994.

(21) (a) Hughes, R. P.; Sweetser, J. T.; Tawa, M. D.; Williamson, A.; Incarvito, C. D.; Rhatigan, B.; Rheingold, A. L.; Rossi, G. *Organometallics* **2001**, *20*, 3800. (b) Hughes, R. P.; Ward, A. J.; Rheingold, A. L.; Zakharov, L. N. *Can. J. Chem.* **2003**, *81*, 1270. (c) Ruddick, J. D.; Shaw, B. L. *J. Chem. Soc. (A)* **1969**, 2969.

(22) Brookhart, M.; Grant, B.; Volpe, J. *Organometallics* **1992**, *11*, 3920.

Scheme 7

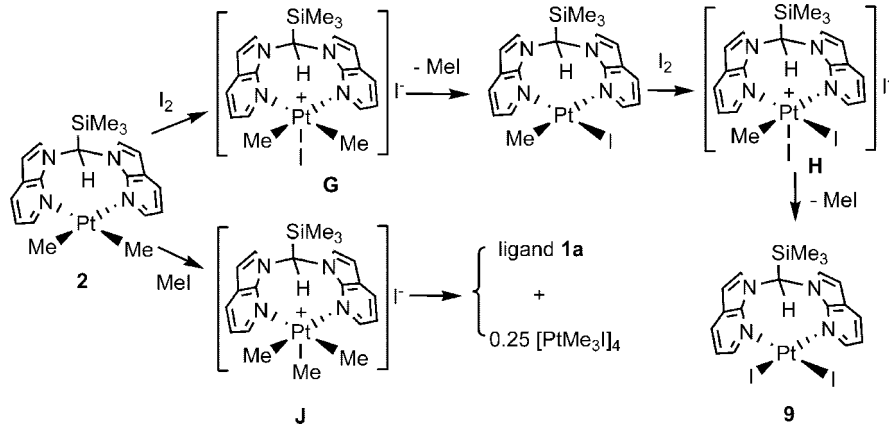

Scheme 8

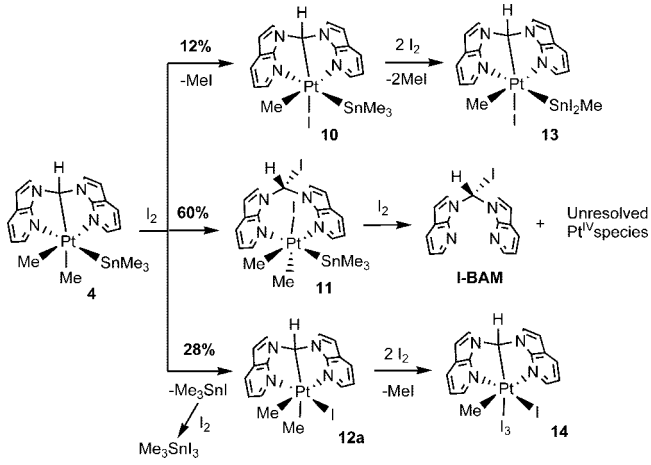

remaining Pt-*Me* group. The I(2)−I(3) bond (3.0669(11) Å) is much longer than the I(3)−I(4) bond (2.7892(12) Å) for the I_3^- anion. In contrast to **M1**,[11] where the axial Pt−C_{BAM} bond (2.143(5) Å) is considerably longer than the basal Pt−CH_3 bonds (2.042(4) Å, in average), the axial Pt(1)−C(16) bond (2.043(11) Å) is much shorter than the basal Pt(1)−C(15) bond (2.146(8) Å) in **14**, while in **13**, the axial and basal Pt−C bonds are nearly identical (2.094(8) and 2.083(8) Å, respectively). The Pt(1)−N(3) (2.086(8) Å) bond in **14** is much shorter than the Pt(1)−N(1) bond (2.177(8) Å), attributable to the stronger trans effect of −Me compared to I^-, while the two Pt−N bond lengths in **13** are similar (Pt(1)−N(1) = 2.160(7) Å, Pt(1)−N(3) = 2.176(7) Å). The observed Pt−C and Pt−N bond length variations in complexes **M1**, **13**, and **14** are consistent with the order of the *trans* effect, −Me > $-Sn(I)_2Me$ > I^-. The N−Pt−N chelating angles in these three compounds vary somewhat (93.21(14)°, 92.2(3)°, and 91.7(3)° for complexes **M1**, **13**, and **14**, respectively).

Reactivity of (*N*,*C*,*N*-BAM)PtMe$_3$ (M1) with I$_2$. To help us understand the reactivity of complex **4** with I_2, a similar reaction with **M1** (Chart 1) was also examined. Addition of 1 equiv of I_2 to a dry CD_2Cl_2 solution of complex **M1** instantly generated a Pt^{IV} complex, (*N*,*C*,*N*-BAM)$PtMe_2$(I) (**12b**) regiospecifically, along with MeI (Scheme 9). Compound **12b** was isolated and fully characterized. It is a geometrical isomer of **12a** with a mirror-plane symmetry according to NMR data (see Figure S18 in the Supporting Information), indicating that the axial Pt-*Me* of **M1** is more reactive than its two basal Pt-*Me*. Unlike **12a** in Scheme 8, the remaining two Me groups in **12b** cannot further react with I_2, as treatment of **12b** with an excess amount of I_2 only gave rise to an I_3^--bonded Pt(IV) complex **15** (Scheme 9), which was characterized by single-crystal X-ray diffraction (see the Supporting Information) and elemental analyses. These facts can be rationalized by the much greater *trans* effect of the BAM methine carbon, compared to the BAM pyridyl. Noteworthy also is that the bridging methine carbon in complex **M1** is insensitive toward I_2 electrophilic attack, but it is involved in one of the major pathways for the reaction of

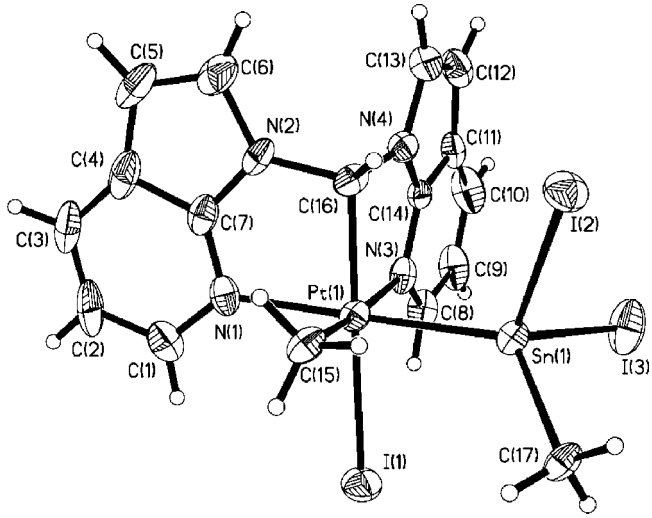

Figure 8. Crystal structure of **13** with 50% thermal ellipsoids and labeling schemes.

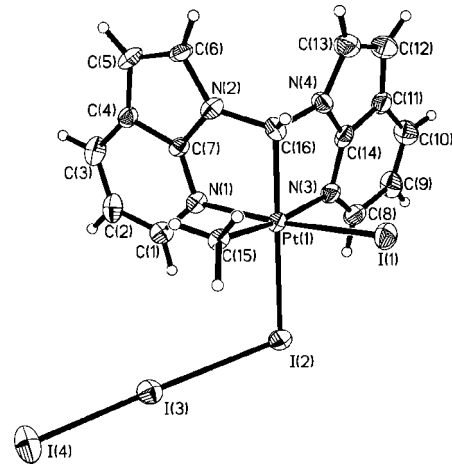

Figure 9. Structure of **14** with 50% thermal ellipsoids and labeling schemes.

Scheme 9

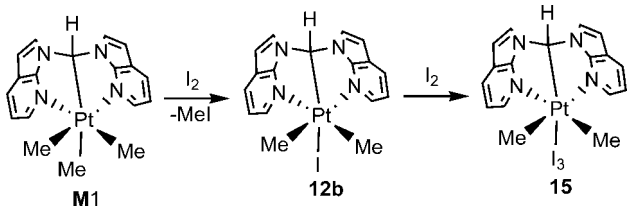

Chart 2

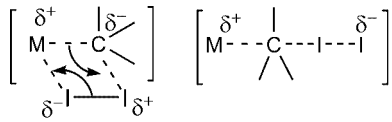

complex **4** with I_2 (Scheme 8). This difference is evidently caused by the $SnMe_3$ group, which perhaps contributes both sterically and electronically to augment the reactivity of the axial $Pt-C_{BAM}$ bond in **4**.

Mechanistic Aspect of the Reactivity of 4 and M1 with I_2. Compared with the prevalent S_N2-reductive functionalization of Pt^{IV}-Me in Shilov chemistry, which occurs via five-coordinate Pt(IV) species and is accompanied by Pt(IV) to Pt(II) conversion,[1,6−9] the reaction behaviors of complexes **4** and **M1** with I_2 are evidently different. To the best of our knowledge, reactivity of coordinatively saturated Pt(IV) complexes, particularly those with multidentate ligands toward electrophiles, remains essentially unexplored. The facile reaction of $Pt^{IV}-C$ bonds with I_2 as shown by **4** and **M1** is rare. We are only aware of one precedent report that describes the cleavage of $Pt^{IV}-C$ bonds using Br_2 and $HgCl_2$.[23] The reactions of **4** and **M1** with I_2 are clearly not initiated by I^- nucleophilic attack since both proved unreactive toward $[Bu_4N]I$. A radical process is also unlikely as light has no obvious effect on the reaction. The heterolytic Pt^{IV}-Me/$SnMe_3$ bond cleavage in **4** and **M1** is most likely initiated with a S_E2 process and proceeds via either a concerted four-membered ring transition state (σ-bond metathesis) or an "opened" polar S_E2 transition state,[23,24] as depicted in Chart 2 (A and B, respectively). The four-membered-ring transition state does not require the preformation of a five-coordinate Pt^{IV} intermediate but generates a quasi seven-coordinate Pt^{IV} species.[24]

The higher reactivity of the basal $Pt-SnMe_3$ bond, compared to the basal Pt−Me bond in **4**, may be caused by the larger size of the Sn atom, making it more susceptible toward initial $I^{\delta+}$ attack. In contrast to **4**, the reduced electron density of the Pt^{IV} center in **10** disfavors the cleavage of its $Pt-SnMe_3$ bond by I_2, thus allowing the competing electrophilic Sn−Me bond cleavage processes. Electrophilic Sn−-Me bond cleavage by I_2 can also occur via transition states as depicted in Chart 2,[25,26] leading to the formation of complex **13**. The remaining Sn−Me bond in **13** is not reactive toward I_2 because of the reduced electron density of its Sn(IV) center.

Conclusions

Novel BAM derivative ligands incorporating Si/Sn functionalities have been successfully developed. These ligands have been demonstrated to exhibit diverse and distinct reactivities with $[PtR_2(\mu\text{-}SMe_2)]_n$ (R = Me, Ph). While the $SiMe_3$ derivative ligand favors the formation of N,N-chelating Pt(II) complexes via ligand displacements, the SnR_3 derivative ligands prefer to undergo $Sn-C_{BAM}$ bond oxidative cleavage, resulting in either *N*,*C*,*N*-chelating Pt(IV) complexes or unexpected products via Sn^{IV}-*Me*/Pt^{II}-*Ph* metathesis. While the steric impact exerted by the $SiMe_3$ group destabilizes the products of Pt(Me_3Si-BAM)Me_2 (**2**) with MeI or MeOTf, it makes a stoichiometric Pt^{II}-Me functionalization of **2** with I_2 possible by preventing the formation of six-coordinate $Pt^{IV}Me_2(I)_2$ species. The reactivity of the *N*,*C*,*N*-chelating Pt(IV) complexes [Pt(*N*,*C*,*N*-BAM)Me_2($SnMe_3$)] (**4**) and [Pt(*N*,*C*,*N*-BAM)Me_3] (**M1**) with I_2 were examined and compared. While the $Pt-C_{BAM}$ bond in complex **M1** is not reactive toward I_2, the basal $SnMe_3$ moiety appears to enhance significantly the reactivity of the $Pt-C_{BAM}$ bond in **4**, and its electrophilic cleavage operates as the major reaction pathway for the reaction of **4** with I_2. We also find that the *trans* effect plays a crucial role in governing the selectivity of the heterolytic Pt^{IV}-Me cleavage processes, whereas the electron-richness of Pt(IV) and Sn(IV) centers has a great impact on the reactivities of the Pt−Sn and Sn−Me bond. The heterolytic Pt^{IV}-Me/$SnMe_3$ or Sn−Me bond cleavage involved for complexes **4**, **M1** or the resulting reaction intermediates may proceed via either a concerted four-membered-ring transition state or an opened polar S_E2 transition state.

Acknowledgment. We thank the Natural Sciences and Engineering Research Council for financial support.

Supporting Information Available: Complete NMR spectra and crystal data for **1a**, **2**, **7**, **9**·**[PtMe$_3$I]$_4$**, **9**·**I$_2$**, and **13**−**15**. This information is available free of charge via the Internet at http://pubs.acs.org.

OM900022N

(23) Roth, S.; Ramamoorthy, V.; Sharp, P. R. *Inorg. Chem.* **1990**, *29*, 3345.

(24) (a) Belluco, U. *Organometallic and Coordination Chemistry of Platinum*; Academic Press: London, 1974. (b) Alibrandi, G.; Minniti, D.; Romeo, R.; Uguagliati, P.; Calligaro, L.; Belluco, U.; Crociani, B. *Inorg. Chim. Acta* **1985**, *100*, 107.

(25) (a) Fukuto, J. M.; Jensen, F. R. *Acc. Chem. Res.* **1983**, *16*, 177. (b) Fukuto, J. M.; Newman, D. A.; Jensen, F. R. *Organometallics* **1987**, *6*, 415, and references therein.

(26) Davies, A. G. *Organotin Chemistry*; VCH: Weinheim, 1997.